Received: 30 June 2023 | Revised: 11 July 2023 | Accepted: 23 August 2023

DOI: 10.1002/pamm.202300171

RESEARCH ARTICLE

Multi-fidelity Gaussian processes for an efficient approximation of frequency sweeps in acoustic problems

Caglar Gurbuz | **Martin Eser** | **Steffen Marburg**

Chair of Vibroacoustics of Vehicles and Machines, Technical University of Munich, Garching, Germany

Correspondence
Caglar Gurbuz, Chair of Vibroacoustics of Vehicles and Machines, Technical University of Munich, Boltzmannstr. 15, 85748 Garching, Germany.
Email: caglar.guerbuez@tum.de

Abstract

This paper presents a multi-fidelity model for the acceleration of frequency sweep analyses in acoustics. In traditional analyses, the frequency-dependent Helmholtz equation is repetitively solved at each frequency. Using the boundary element method requires then a plethora of evaluations resulting in high computational costs. In the proposed method, the fidelity levels are realized as Gaussian processes, which are conditioned on observations obtained by boundary element simulations. A coarse boundary element mesh is considered as the low-fidelity model, whereas a fine mesh is adopted as the high-fidelity model. To validate the proposed framework, the vehicle interior noise problem is investigated. The results demonstrate that multi-fidelity Gaussian processes efficiently accelerate the frequency sweep analysis, as they provide accurate and fast predictions across the entire frequency range of interest. As a beneficial side effect, the present method takes uncertainties into account. This allows to consider limited information on the model, which is particularly important in early design phases.

1 | INTRODUCTION

With rising demands on modern acoustic systems, the underlying design processes rely on accurate and fast predictions of the system behavior at early stages. However, accurate models are usually computationally costly. In contrast to this, fast-to-solve models are generally insufficient in terms of accuracy. Particularly in time-harmonic acoustics, the design of an acoustic system is evaluated across a certain frequency range. This type of study is usually referred to as frequency sweep analysis. In traditional studies with the boundary element method (BEM), this frequency sweep is performed by repetitively solving the associated system at each relevant frequency. Recent research, thus, focuses on acceleration techniques to improve the efficiency in frequency sweep analyses. For instance, a greedy reduced basis [1–3] or parametric model order reduction methods [4–7] have been developed. The interested reader is referred to [8] for a thorough review in this area. These existing techniques, however, do not account for uncertainties eventually occurring in the design process. In the field of automotive interior acoustics, the efficient evaluation under uncertainties plays a crucial role in the early design phase, as the model parameters are not definitively determined at this stage [9–11].

The multi-fidelity formulation based on Gaussian processes (GPs) can be traced back to Kennedy and O'Hagan [12]. Their model has been extended for several fidelity levels by Le Gratiet and Garnier [13]. Recent research in this field focuses on solutions of partial differential equations [14] and random fields [15]. As an alternative to GPs, neural networks

have been incorporated in multi-fidelity models [16, 17] allowing discontinuities between the fidelity models [16]. Neural network-based multi-fidelity models have been further applied in the field of structural health monitoring [18]. The advantage of using GP surrogates is that they allow to combine the experts intuition in a probabilistic manner [19, 20]. In recent years, GPs have been developed for the treatment of linear [21] and nonlinear partial differential equations [22]. In acoustics, GPs have been applied as surrogate for chassis transfer path analysis [23], for the reconstruction of a sound field [24], and for the localization of sources in the ocean [25, 26].

2 | BEM

The time-harmonic acoustic problem is governed by the Helmholtz equation, which can be expressed for three-dimensional problems by

$$\Delta p(\vec{\boldsymbol{x}}) + k^2 p(\vec{\boldsymbol{x}}) = 0 \qquad \vec{\boldsymbol{x}} \in \Omega \subset \mathbb{R}^3, \tag{1}$$

where $p(\vec{\boldsymbol{x}})$ denotes the sound pressure in the computational domain Ω. The parameter $k = 2\pi f/c$ denotes the wavenumber where f and c represent frequency and speed of sound. In this work, we focus on sound waves propagating in air. Consequently, we refer to $c = c_a$ and $\rho = \rho_a$ as the speed of sound and the density of air. The solution of the Helmholtz equation needs to satisfy the Robin boundary condition on Γ, which is expressed by [27]

$$v_f(\vec{\boldsymbol{x}}) - v_s(\vec{\boldsymbol{x}}) = Y(\vec{\boldsymbol{x}}) p(\vec{\boldsymbol{x}}) \qquad \vec{\boldsymbol{x}} \in \Gamma \subset \mathbb{R}^2. \tag{2}$$

The normal fluid particle velocity, the normal structural velocity, and the boundary admittance are denoted by $v_f(\vec{\boldsymbol{x}})$, $v_s(\vec{\boldsymbol{x}})$, and $Y(\vec{\boldsymbol{x}})$, respectively. In computational acoustics, Robin boundary conditions are of great importance, as they allow to incorporate absorbing properties within the numerical model. Discretizing the weak formulation of the Helmholtz equation with the collocation method yields the Kirchhoff-Helmholtz boundary integral equation, which is formulated as

$$c(\vec{\boldsymbol{y}}) p(\vec{\boldsymbol{y}}) + \int_\Gamma \frac{\partial G(\vec{\boldsymbol{x}}, \vec{\boldsymbol{y}})}{\partial n(\vec{\boldsymbol{x}})} p(\vec{\boldsymbol{x}}) \mathrm{d}\Gamma(\vec{\boldsymbol{x}}) = \mathrm{i}\omega\rho_a \int_\Gamma G(\vec{\boldsymbol{x}}, \vec{\boldsymbol{y}}) v_f(\vec{\boldsymbol{x}}) \mathrm{d}\Gamma(\vec{\boldsymbol{x}}), \tag{3}$$

where $G(\vec{\boldsymbol{x}}, \vec{\boldsymbol{y}}) = \mathrm{e}^{\mathrm{i}kr}/(4\pi r)$ with $r = r(\vec{\boldsymbol{x}}, \vec{\boldsymbol{y}})$ represents the three-dimensional Green's function. The integral-free term $c(\vec{\boldsymbol{y}})$ is specified by the shape of the boundary at the position $\vec{\boldsymbol{y}}$. In this study, we use discontinuous BEMs leading to collocation points, which are placed inside the boundary element. As a consequence, the collocation points are located on smooth parts of the boundary resulting in $c(\vec{\boldsymbol{y}}) = 0.5$ [28]. In a final step, we apply polynomial approximation functions yielding the linear system of equations for the BEM

$$[\boldsymbol{H}(k) - \boldsymbol{G}(k)\boldsymbol{Y}(k)]\boldsymbol{p}(k) = \boldsymbol{G}(k)\boldsymbol{v}_s(k) \tag{4}$$

with $\boldsymbol{G}(k)$ and $\boldsymbol{H}(k)$ representing the boundary element system matrices. They are neither Hermitian nor positive definite. Note that the solution of the acoustic problem $\boldsymbol{p}(k)$ is depending on k and, thus, on the frequency. As a consequence, frequency sweep analyses of acoustic systems require a large number of evaluations of the linear system of equations in Equation (4). Once we obtain the sound pressure solution on the boundary, the sound pressure at a field point located in Ω can be evaluated by

$$p_i(\vec{\boldsymbol{y}}) = \mathrm{i}\omega\rho_a \int_\Gamma G(\vec{\boldsymbol{x}}, \vec{\boldsymbol{y}}) v_s(\vec{\boldsymbol{x}}) \mathrm{d}\Gamma(\vec{\boldsymbol{x}}) - \int_\Gamma \left[\frac{\partial G(\vec{\boldsymbol{x}}, \vec{\boldsymbol{y}})}{\partial n(\vec{\boldsymbol{x}})} - \mathrm{i}\omega\rho_a G(\vec{\boldsymbol{x}}, \vec{\boldsymbol{y}}) Y(\vec{\boldsymbol{x}}) \right] p(\vec{\boldsymbol{x}}) \mathrm{d}\Gamma(\vec{\boldsymbol{x}}) \qquad \vec{\boldsymbol{y}} \in \Omega \tag{5}$$

with the subscript i denoting the acoustic quantity evaluated at an internal field point.

3 | MULTI-FIDELITY GAUSSIAN PROCESS

The aforementioned BEM is used to solve the Helmholtz equation in three spatial directions for a single frequency. This results in a system response, designated by the sound pressure level at the driver's position, at a single frequency. To approximate the system response in the dimension of the frequency, GPs are introduced. In general terms, a GP

$$h(\mathbf{f}) \sim \mathcal{GP}\big(m(\mathbf{f}), \mathrm{cov}(\mathbf{f}, \mathbf{f}')\big) \tag{6}$$

can be viewed as a probability distribution over functions. It is specified by its mean $m(\mathbf{f})$ and covariance function $\mathrm{cov}(\mathbf{f}, \mathbf{f}')$ with $\mathbf{f}$ and $\mathbf{f}'$ denoting two frequency sets [21]. In literature, the covariance functions is commonly referred to as kernel. In this work, the squared exponential kernel is chosen as the covariance function

$$\mathrm{cov}(\mathbf{f}, \mathbf{f}') = \sigma_f^2 \, \exp\left(-\frac{1}{2l^2}(\mathbf{f} - \mathbf{f}')^T(\mathbf{f} - \mathbf{f}')\right), \tag{7}$$

where l and σ_f^2 refer to the characteristic length and the signal variance σ_f^2. As these two parameters mainly determine the behavior of a GP, they are also referred to as hyperparameters. It should be highlighted that the covariance of the output responses is solely determined by the covariance of the input frequencies. Increasing distances between the input frequencies thus result in a decreased covariance of the outputs [19]. Prior to the incorporation of observed responses, a GP is defined by

$$\mathbf{h} \sim \mathcal{N}\big(\mathbf{0}, \mathrm{cov}(\mathbf{f}, \mathbf{f}')\big) \tag{8}$$

with $\mathcal{N}$ representing a multivariate Gaussian normal distribution. For practical reasons, the mean function is set zero. The GP without any observed data is usually called GP prior. Now, by considering observations on the system response, the joint probability distribution of the observed function outputs $\mathbf{h}$ and the unknown frequency responses $\mathbf{h}_*$ at the frequencies of interest $\mathbf{f}_*$ is formulated as

$$\begin{bmatrix} \mathbf{h} \\ \mathbf{h}_* \end{bmatrix} \sim \mathcal{N}\left(\mathbf{0}, \begin{bmatrix} \mathbf{K}(\mathbf{f}, \mathbf{f}) & \mathbf{K}(\mathbf{f}, \mathbf{f}_*) \\ \mathbf{K}(\mathbf{f}_*, \mathbf{f}) & \mathbf{K}(\mathbf{f}_*, \mathbf{f}_*) \end{bmatrix}\right). \tag{9}$$

The covariance matrix $\mathbf{K}$ is assembled by evaluating the kernel for the combination of the two frequency sets, $\mathbf{f}$ and $\mathbf{f}_*$. For n frequencies with observed response functions and n_* frequencies with unobserved responses, $\mathbf{K}(\mathbf{f}, \mathbf{f})$, $\mathbf{K}(\mathbf{f}_*, \mathbf{f})$, and $\mathbf{K}(\mathbf{f}_*, \mathbf{f}_*)$ are of size $n \times n$, $n_* \times n$, and $n_* \times n_*$, respectively. By computing the Schur complement, the joint posterior probability distribution for the response functions of interest can be formulated as

$$P(\mathbf{h}_*|\mathbf{f}_*, \mathbf{f}, \mathbf{h}) \sim \mathcal{N}(\mathbf{K}(\mathbf{f}_*, \mathbf{f})\mathbf{K}(\mathbf{f}, \mathbf{f})^{-1}\mathbf{h}, \mathbf{K}(\mathbf{f}_*, \mathbf{f}_*) - \mathbf{K}(\mathbf{f}_*, \mathbf{f})\mathbf{K}(\mathbf{f}, \mathbf{f})^{-1}\mathbf{K}(\mathbf{f}, \mathbf{f}_*)). \tag{10}$$

Up to now, the presence of noise in the data has been neglected. By assuming independently distributed Gaussian noise, noisy versions of the observations $\mathbf{y}$ can be included according to $\mathbf{y} = \mathbf{h}(\mathbf{f}) + \epsilon$. In that case, the covariance function is expressed by

$$\mathrm{cov}(\mathbf{f}, \mathbf{f}') = \mathbf{K}(\mathbf{f}, \mathbf{f}) + \sigma_n^2\mathbf{I}, \tag{11}$$

where σ_n^2 and $\mathbf{I}$ denote the level of noise and the identity matrix, respectively. For noisy observations, the joint probability distribution reads

$$\begin{bmatrix} \mathbf{y} \\ \mathbf{h}_* \end{bmatrix} \sim \mathcal{N}\left(\mathbf{0}, \begin{bmatrix} \mathbf{K}(\mathbf{f}, \mathbf{f}) + \sigma_n^2\mathbf{I} & \mathbf{K}(\mathbf{f}, \mathbf{f}_*) \\ \mathbf{K}(\mathbf{f}_*, \mathbf{f}) & \mathbf{K}(\mathbf{f}_*, \mathbf{f}_*) \end{bmatrix}\right). \tag{12}$$

Again, computing the Schur complement yields the posterior GP in the presence of noise

$$P(\mathbf{h}_*|\mathbf{f}_*, \mathbf{f}, \mathbf{y}) \sim \mathcal{N}\big(\bar{\mathbf{h}}_*, \mathrm{cov}(\mathbf{h}_*)\big), \tag{13}$$

with the posterior mean $\bar{\mathbf{h}}_*$ and the posterior covariance function $\mathrm{cov}(\mathbf{h}_*)$

$$\bar{\mathbf{h}}_* = \mathbf{K}(\mathbf{f}_*, \mathbf{f})\left[\mathbf{K}(\mathbf{f}, \mathbf{f}) + \sigma_n^2 \mathbf{I}\right]^{-1} \mathbf{y}, \tag{14}$$

$$\mathrm{cov}(\mathbf{h}_*) = \mathbf{K}(\mathbf{f}_*, \mathbf{f}_*) - \mathbf{K}(\mathbf{f}_*, \mathbf{f})\left[\mathbf{K}(\mathbf{f}, \mathbf{f}) + \sigma_n^2 \mathbf{I}\right]^{-1} \mathbf{K}(\mathbf{f}, \mathbf{f}_*)^T. \tag{15}$$

At this point, the posterior GP can be readily applied as a surrogate for the approximation of acoustic system responses [19]. Lastly, the parameters of the covariance function are determined by minimizing the negative log likelihood function [19]

$$\log P(\mathbf{y}|\mathbf{f}) = -\frac{1}{2}\mathbf{y}^T(\mathbf{K}(\mathbf{f}, \mathbf{f}) + \sigma_n^2 \mathbf{I}))\mathbf{y} - \frac{1}{2}\log|\mathbf{K}(\mathbf{f}, \mathbf{f}) + \sigma_n^2 \mathbf{I}| - \frac{n}{2}\log 2\pi \tag{16}$$

Turning now to the multi-fidelity GP, the solution of a high-fidelity model can be approximated by a lower fidelity solution [12]. Kennedy and O'Hagan refer to that type as auto-regressive multi-fidelity model. An auto-regressive multi-fidelity model with two levels is formulated as

$$\mathbf{h}_H(\mathbf{f}) = \eta\, \mathbf{h}_L(\mathbf{f}) + \delta(\mathbf{f}), \tag{17}$$

where $\mathbf{h}_L$ and δ represent two independent GPs

$$\mathbf{h}_L \sim \mathcal{GP}\left(0, \mathrm{cov}_L\left(\mathbf{f}, \mathbf{f}'\right)\right) \tag{18}$$

$$\delta \sim \mathcal{GP}\left(0, \mathrm{cov}_H\left(\mathbf{f}, \mathbf{f}'\right)\right). \tag{19}$$

The coupling between the levels is established by the parameter η. It becomes clear that the fidelity levels are uncorrelated when $\eta = 0$. In that case, the multi-fidelity will not yield any improvements [16]. The subscripts L and H are introduced in order to refer to the low-fidelity and the high-fidelity level. Analogously, the multi-fidelity GP prior is expressed by

$$\begin{bmatrix}\mathbf{h}_L \\ \mathbf{h}_H\end{bmatrix} \sim \mathcal{GP}\left(\begin{bmatrix}\mathbf{0} \\ \mathbf{0}\end{bmatrix}, \begin{bmatrix}\mathrm{cov}_L(\mathbf{f}_L, \mathbf{f}_L) & \eta\,\mathrm{cov}_L(\mathbf{f}_L, \mathbf{f}_H) \\ \eta\,\mathrm{cov}_L(\mathbf{f}_L, \mathbf{f}_H) & \eta^2\,\mathrm{cov}_L(\mathbf{f}_L, \mathbf{f}_H) + \mathrm{cov}_H(\mathbf{f}_L, \mathbf{f}_H)\end{bmatrix}\right). \tag{20}$$

By summarizing the kernel expressions as $\mathrm{cov}_{LL} = \mathrm{cov}_L$, $\mathrm{cov}_{LH} = \mathrm{cov}_{HL} = \eta\,\mathrm{cov}_L$, and $\mathrm{cov}_{HH} = \eta^2\,\mathrm{cov}_L + \mathrm{cov}_H$, Equation (20) can be rearranged to

$$\begin{bmatrix}\mathbf{h}_L \\ \mathbf{h}_H\end{bmatrix} \sim \mathcal{GP}\left(\begin{bmatrix}\mathbf{0} \\ \mathbf{0}\end{bmatrix}, \begin{bmatrix}\mathrm{cov}_{LL}(\mathbf{f}_L, \mathbf{f}_L) & \mathrm{cov}_{LH}(\mathbf{f}_L, \mathbf{f}_H) \\ \mathrm{cov}_{HL}(\mathbf{f}_L, \mathbf{f}_H) & \mathrm{cov}_{HH}(\mathbf{f}_L, \mathbf{f}_H)\end{bmatrix}\right). \tag{21}$$

By taking the response functions of interest into account, the joint probability distribution for multi-fidelity model reads

$$\begin{bmatrix}\mathbf{h}_* \\ \mathbf{h}_L \\ \mathbf{h}_H\end{bmatrix} \sim \mathcal{GP}\left(\begin{bmatrix}\mathbf{0} \\ \mathbf{0} \\ \mathbf{0}\end{bmatrix}, \begin{bmatrix}\mathrm{cov}_{**}(\mathbf{f}_*, \mathbf{f}_*) & \mathrm{cov}_{*L}(\mathbf{f}_*, \mathbf{f}_L) & \mathrm{cov}_{*H}(\mathbf{f}_*, \mathbf{f}_H) \\ \mathrm{cov}_{L*}(\mathbf{f}_L, \mathbf{f}_*) & \mathrm{cov}_{LL}(\mathbf{f}_L, \mathbf{f}_L) & \mathrm{cov}_{LH}(\mathbf{f}_L, \mathbf{f}_H) \\ \mathrm{cov}_{H*}(\mathbf{f}_H, \mathbf{f}_*) & \mathrm{cov}_{HL}(\mathbf{f}_L, \mathbf{f}_H) & \mathrm{cov}_{HH}(\mathbf{f}_H, \mathbf{f}_H)\end{bmatrix}\right). \tag{22}$$

The computation of the Schur complement then leads to the multi-fidelity GP posterior

$$P(\mathbf{h}_*|\mathbf{f}_*, \mathbf{f}_L, \mathbf{h}_L, \mathbf{f}_H, \mathbf{h}_H) = \mathcal{N}(\mathbf{K}_*\mathbf{K}^{-1}\mathbf{h}, \mathbf{K}_{**} - \mathbf{K}_*\mathbf{K}^{-1}\mathbf{K}_*^T), \tag{23}$$

where

$$\mathbf{h} = \begin{bmatrix}\mathbf{h}_L & \mathbf{h}_H\end{bmatrix}^T, \tag{24}$$

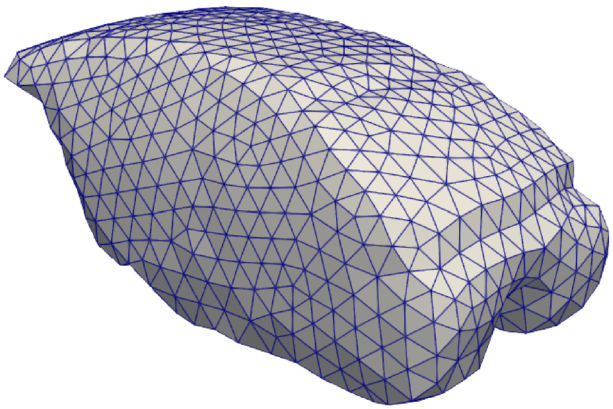

FIGURE 1 Boundary element mesh of a vehicle cabin for the low fidelity level. The low fidelity mesh consists of 1906 degrees of freedom.

$$\mathbf{K}_* = \begin{bmatrix} \mathrm{cov}_{*L}(\mathbf{f}_*, \mathbf{f}_L) & \mathrm{cov}_{*H}(\mathbf{f}_*, \mathbf{f}_H) \end{bmatrix}, \tag{25}$$

$$\mathbf{K} = \begin{bmatrix} \mathrm{cov}_{LL}(\mathbf{f}_L, \mathbf{f}_L) & \mathrm{cov}_{LH}(\mathbf{f}_L, \mathbf{f}_H) \\ \mathrm{cov}_{HL}(\mathbf{f}_H, \mathbf{f}_L) & \mathrm{cov}_{HH}(\mathbf{f}_H, \mathbf{f}_H) \end{bmatrix}, \tag{26}$$

$$\mathbf{K}_{**} = \begin{bmatrix} \mathrm{cov}_{**}(\mathbf{f}_*, \mathbf{f}_*) \end{bmatrix}. \tag{27}$$

Similarly, the multi-fidelity GP posterior for noisy frequency responses, $\mathbf{y}_L$ and $\mathbf{y}_H$, can be formulated as

$$P(\mathbf{h}_*|\mathbf{f}_*, \mathbf{f}_L, \mathbf{y}_L, \mathbf{f}_H, \mathbf{f}_H) = \mathcal{N}(\mathbf{K}_*\mathbf{K}^{-1}\mathbf{y}, \mathbf{K}_{**} - \mathbf{K}_*\mathbf{K}^{-1}\mathbf{K}_*^T) \tag{28}$$

with $\mathbf{y} = [\mathbf{y}_L \ \mathbf{y}_H]$. In this case, the covariance matrix is modified to

$$\mathbf{K} = \begin{bmatrix} \mathrm{cov}_{LL}(\mathbf{f}_L, \mathbf{f}_L) + \sigma_{nL}^2\mathbf{I} & \mathrm{cov}_{LH}(\mathbf{f}_L, \mathbf{f}_H) \\ \mathrm{cov}_{HL}(\mathbf{f}_H, \mathbf{f}_L) & \mathrm{cov}_{HH}(\mathbf{f}_H, \mathbf{f}_H) + \sigma_{nH}^2\mathbf{I} \end{bmatrix}, \tag{29}$$

with σ_{nL}^2 and σ_{nH}^2 denoting the noise levels related to the fidelity levels. Another way to quantify noise is the signal-to-noise ratio (SNR), which can be expressed by

$$\mathrm{SNR} = 10 \cdot \log(\frac{\mathbf{y}\,\mathbf{y}^T}{\sigma_n^2}). \tag{30}$$

The parameters of the kernels are again obtained by minimizing the negative log likelihood function. For the multi-fidelity model, the negative log likelihood function reads

$$\log P(\mathbf{y}|\mathbf{f}) = -\frac{1}{2}\mathbf{y}^T\left[\mathbf{K}(\mathbf{f},\mathbf{f}) + \sigma_n^2\mathbf{I}\right]^{-1}\mathbf{y} - \frac{1}{2}\log|\mathbf{K}(\mathbf{f},\mathbf{f}) + \sigma_n^2\mathbf{I}| - \frac{n_L + n_H}{2}\log 2\pi. \tag{31}$$

For more details on the formulation of the algorithm, the interested reader is referred to [29].

4 | NUMERICAL EXAMPLE

A rather coarse boundary element mesh is considered as the low-fidelity level, while a fine mesh is regarded as the high-fidelity model. The low-fidelity mesh consists of 1906 degrees of freedom, whereas the high-fidelity mesh has 24036, see Figure 1 and Figure 2. Regarding the frequency response function, the sound pressure level is evaluated at the position of

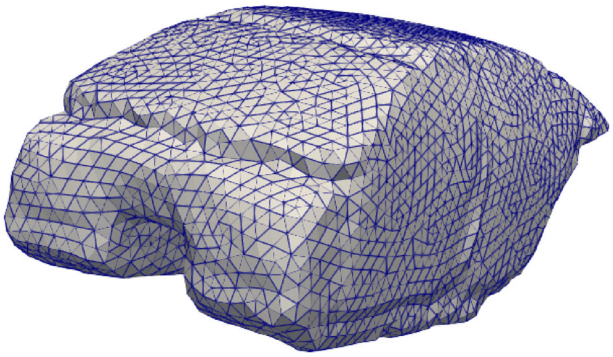

FIGURE 2 Boundary element mesh of a vehicle cabin for the high fidelity level. The high fidelity mesh consists of 24 036 degrees of freedom.

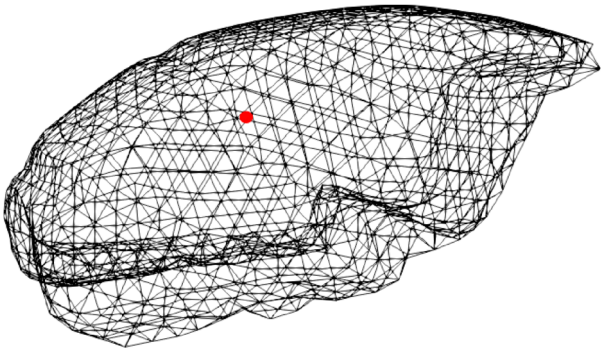

FIGURE 3 Field point at which the sound pressure level is evaluated. The field point is chosen at the position of the driver's ear.

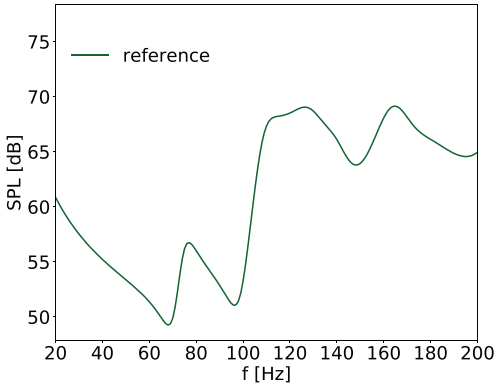

FIGURE 4 Reference sound pressure level from 20 to 200 Hz (green). This response is obtained by evaluating the high fidelity boundary element model at each discrete frequency.

the driver's ear, see Figure 3. The reference sound pressure is chosen as $p_{\text{ref}} = 2.0 \cdot 10^{-5}$ Pa.

In Figure 4 to 7, the entire multi-fidelity procedure is depicted. Prior to the multi-fidelity approximation, the reference solution is investigated (Figure 4). The reference solution is obtained by solving the boundary element system at each frequency. In the initial step, the low-fidelity approximation is computed for two reasons: First, to gain initial insights on the system behavior, and second, to estimate those frequencies, at which the evaluation of the high-fidelity system is required. The relevant frequencies are chosen in a relatively empirical way. The frequencies with the maxima in the frequency response and in the curvatures of the low-fidelity solutions are designated as the frequencies for the high-fidelity simulations. Then, the high-fidelity system is solved at the selected frequencies (Figure 6). In the final step, the multi-fidelity approximation is computed. Overall, the comparison with the reference solution shows that the multi-fidelity approximation is in good agreement with the reference solution. Small deviations solely occur around 130 to 140 Hz.

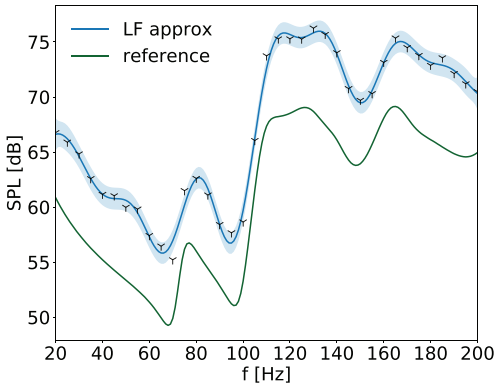

FIGURE 5 Reference solution (green) and the low fidelity approximation from 20 to 200 Hz. The low-fidelity approximation is specified by the posterior mean (blue) and the posterior covariance corresponding to the 95% confidence interval (light blue shaded). The Y-shaped markers denote the frequency responses of the low fidelity model.

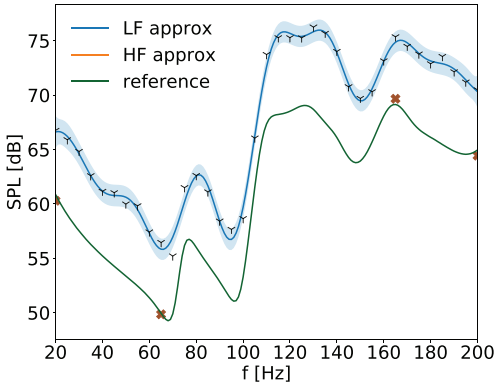

FIGURE 6 Reference solution (green) and the low fidelity approximation (posterior mean: blue, posterior covariance: light blue) from 20 to 200 Hz. The solution of the high fidelity boundary element model is obtained at four frequencies (orange crosses).

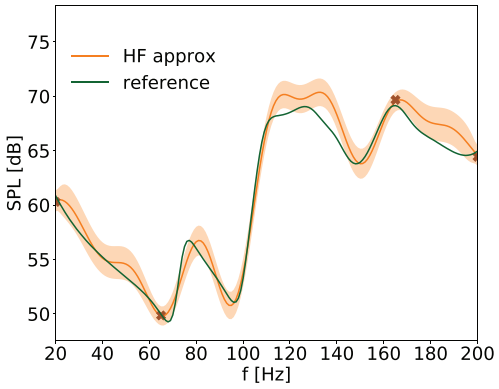

FIGURE 7 Approximation of the multi-fidelity Gaussian process (orange) and the high-fidelity reference solution (green) from 20 to 200 Hz. The high-fidelity approximation is specified by its posterior mean (orange) and the posterior covariance corresponding to the 95% confidence interval (light orange shaded).

Regarding the computational time, the reference solution is obtained in 48.52 h, while the approximation required 1.39 h. Thus, the proposed method serves as an efficient tool for frequency sweep analyses.

5 | CONCLUSIONS

This work set out to explore the capabilities of multi-fidelity models in terms of accelerated frequency sweeps. The multi-fidelity model in this study is composed of two levels. These levels correspond to two boundary element meshes, where the coarser mesh is regarded as the low-fidelity model and the fine mesh as the high-fidelity model. In this multi-fidelity scheme, Gaussian processes are used as surrogates. The findings in this study highlight that multi-fidelity models can be effectively applied for accelerated frequency sweep analyses, as they enable efficient and robust approximations. Since this study has focused only on linear correlated fidelity levels, future work should address the extension to nonlinear correlation functions.

ACKNOWLEDGMENTS

Open access funding enabled and organized by Projekt DEAL.

ORCID

Caglar Gurbuz https://orcid.org/0000-0001-8669-8371

REFERENCES

1. Baydoun, S. K., Voigt, M., Jelich, C., & Marburg, S. (2020). A greedy reduced basis scheme for multifrequency solution of structural acoustic systems. *International Journal for Numerical Methods in Engineering*, *121*(2), 187–200.
2. Baydoun, S. K., Voigt, M., & Marburg, S. (2021). Low-rank iteration schemes for the multi-frequency solution of acoustic boundary element equations. *Journal of Theoretical and Computational Acoustics*, *29*(03), 2150004.
3. Jelich, C., Koji Baydoun, S., Voigt, M., & Marburg, S. (2021). A greedy reduced basis algorithm for structural acoustic systems with parameter and implicit frequency dependence. *International Journal for Numerical Methods in Engineering*, *122*(24), 7409–7430.
4. Panagiotopoulos, D., Desmet, W., & Deckers, E. (2022). Parametric model order reduction for acoustic boundary element method systems through a multiparameter Krylov subspaces recycling strategy. *International Journal for Numerical Methods in Engineering*, *123*, 5546–5569.
5. Xie, X., & Liu, Y. (2021). Efficient multi-frequency solutions of fe–be coupled structural–acoustic problems using Arnoldi-based dimension reduction approach. *Computer Methods in Applied Mechanics and Engineering*, *386*, 114126.
6. Xie, X., Wang, W., He, K., & Li, G. (2022). Fast model order reduction boundary element method for large-scale acoustic systems involving surface impedance. *Computer Methods in Applied Mechanics and Engineering*, *400*, 115618.
7. Xie, X., Zuo, Q., Chen, H., Xu, Y., Yi, Z., & He, K. (2022). A non-intrusive model order reduction boundary element method for frequency sweeps of 2D acoustics. *Journal of Sound and Vibration*, *544*, 117396.
8. Preuss, S., Gurbuz, C., Jelich, C., Baydoun, S. K., & Marburg, S. (2022). Recent advances in acoustic boundary element methods. *Journal of Theoretical and Computational Acoustics*, *30*(03), 2240002.
9. Gurbuz, C., Schmid, J. D., Luegmair, M., & Marburg, S. (2022). Energy density-based non-negative surface contributions in interior acoustics. *Journal of Sound and Vibration*, *527*, 116824.
10. Gurbuz, C., & Marburg, S. (2022). Efficient analysis of energy-based surface contributions for an entire acoustic cavity. *Journal of Theoretical and Computational Acoustics*.
11. Schmid, J. D., Hildenbrand, A., Gurbuz, C., Luegmair, M., & Marburg, S. (2022). Variational autoencoders for dimensionality reduction of automotive vibroacoustic models. *SAE International Journal of Advances and Current Practices in Mobility*, *5*, 830–0838.
12. Kennedy, M. C., & O'Hagan, A. (2000). Predicting the output from a complex computer code when fast approximations are available. *Biometrika*, *87*(1), 1–13.
13. Le Gratiet, L., & Garnier, J. (2014). Recursive co-kriging model for design of computer experiments with multiple levels of fidelity. *International Journal for Uncertainty Quantification*, *4*(5), 1–24.
14. Raissi, M., Perdikaris, P., & Karniadakis, G. E. (2017). Inferring solutions of differential equations using noisy multi-fidelity data. *Journal of Computational Physics*, *335*, 736–746.
15. Parussini, L., Venturi, D., Perdikaris, P., & Karniadakis, G. E. (2017). Multi-fidelity gaussian process regression for prediction of random fields. *Journal of Computational Physics*, *336*, 36–50.
16. Raissi, M., & Karniadakis, G. (2016). Deep multi-fidelity gaussian processes. *arXiv preprint arXiv:1604.07484*.
17. Guo, M., Manzoni, A., Amendt, M., Conti, P., & Hesthaven, J. S. (2022). Multi-fidelity regression using artificial neural networks: Efficient approximation of parameter-dependent output quantities. *Computer methods in applied mechanics and engineering*, *389*, 114378.
18. Torzoni, M., Manzoni, A., & Mariani, S. (2023). A deep neural network, multi-fidelity surrogate model approach for Bayesian model updating in SHM. *European Workshop on Structural Health Monitoring*, *2*, 1076-1086.
19. Williams, C. K., & Rasmussen, C. E. (2006). *Gaussian processes for machine learning*, MIT press Cambridge.
20. Cutajar, K., Pullin, M., Damianou, A., Lawrence, N., & González, J. (2019). Deep gaussian processes for multi-fidelity modeling. *arXiv preprint arXiv:1903.07320*.
21. Raissi, M., Perdikaris, P., & Karniadakis, G. E. (2017). Machine learning of linear differential equations using Gaussian processes. *Journal of Computational Physics*, *348*, 683–693.

22. Raissi, M., Perdikaris, P., & Karniadakis, G. E. (2018). Numerical Gaussian processes for time-dependent and nonlinear partial differential equations. *SIAM Journal on Scientific Computing*, *40*(1), A172–A198.
23. Gurbuz, C., Eser, M., Schmid, J. D., Marburg, S., & Luegmair, M. (2022). Gaussian processes for transfer path analysis applied on vehicle body vibration problems. *SAE International Journa of Advances and Current Practices in Mobility*, *5*, 860–8650.
24. Caviedes-Nozal, D., Riis, N. A., Heuchel, F. M., Brunskog, J., Gerstoft, P., & Fernandez-Grande, E. (2021). Gaussian processes for sound field reconstruction. *The Journal of the Acoustical Society of America*, *149*(2), 1107–1119.
25. Michalopoulou, Z. H., Gerstoft, P., & Caviedes-Nozal, D. (2021). Matched field source localization with gaussian processes. *JASA Express Letters*, *1*(6), 064801.
26. Michalopoulou, Z. H., & Gerstoft, P. (2022). Uncertainty reduction in matched field inversion using gaussian processes. *The Journal of the Acoustical Society of America*, *151*(4), A66–A66.
27. Suzuki, S., Maruyama, S., & Ido, H. (1989). Boundary element analysis of cavity noise problems with complicated boundary conditions. *Journal of Sound and Vibration*, *130*(1), 79–96.
28. Marburg, S. (2018). *Boundary element method for time-harmonic acoustic problems*. Springer.
29. Gurbuz, C., Eser, M., Schaffner, J., & Marburg, S. (2023). A multi-fidelity gaussian process for efficient frequency sweeps in the acoustic design of a vehicle cabin. *The Journal of the Acoustical Society of America*, *153*(4), 2006–2006.

How to cite this article: Gurbuz, C., Eser, M., and Marburg, S. (2023). Multi-fidelity Gaussian processes for an efficient approximation of frequency sweeps in acoustic problems. *Proceedings in Applied Mathematics and Mechanics*, *23,* e202300171. https://doi.org/10.1002/pamm.202300171